Combustion and Flame 262 (2024) 113373

Contents lists available at ScienceDirect

Combustion and Flame

journal homepage: www.sciencedirect.com/journal/combustion-and-flame

Combustion behavior of aluminized metal iodate composites. Part 2: Iodine and energy release rate

Yujie Wang, George Issac Paul, Erik Hagen, Haiyang Wang, Michael R. Zachariah *

University of California, Riverside, CA 92521, United States

ARTICLE INFO

Keywords:
Metal iodate
Thermite
3D printing
Combustion
Iodine release
Energy release

ABSTRACT

Metal iodates are attractive oxidizers in the biocidal application due to their high oxygen and iodine content. In this study, we systematically investigate the iodine release, ignition, and reactivity of aluminized alkali and alkaline metal iodate thermites, namely Al-$Mg(IO_3)_2$, Al-$Ca(IO_3)_2$, Al-$LiIO_3$, Al-$NaIO_3$ and Al-KIO_3, as well as the combustion behavior of assembled high-loading aluminized metal iodate composites. Temperature-jump/time-of-flight mass spectrometry (T-Jump/TOFMS) results demonstrate that Al-$Mg(IO_3)_2$, Al-$Ca(IO_3)_2$, and Al-$LiIO_3$ release a substantial amount of iodine at approximately the same temperature, whereas Al-$NaIO_3$ and Al-KIO_3 exhibit minimal iodine release. In contrast, combustion cell result reveals that the reactivity of Al-$Mg(IO_3)_2$, Al-$Ca(IO_3)_2$, and Al-$LiIO_3$ is lower than Al-$NaIO_3$ and Al-KIO_3, indicating a trade-off between iodine release and reactivity among aluminized metal iodates. Iodine release rate, derived from the combination of T-Jump TOFMS and combustion cell data, reveals that Al-$Mg(IO_3)_2$ and Al-$Ca(IO_3)_2$ have significantly higher iodine release rates than Al-$LiIO_3$. Free-standing Al-metal iodate composites with nearly 50 wt% iodine content are successfully assembled by 3D printing and their combustion behaviors are characterized by high-speed videography and pyrometry for flame temperature measurement. It is found that only Al-$Ca(IO_3)_2$, Al-$LiIO_3$ and Al-$NaIO_3$ achieve complete propagation in an inert environment, and their microscopic combustion characteristics are similar. The propagation rate and flame temperature of Al-$Ca(IO_3)_2$ and Al-$LiIO_3$ are lower than Al-$NaIO_3$, resulting in a higher energy release rate of Al-$NaIO_3$ compared to Al-$Ca(IO_3)_2$ and Al-$LiIO_3$, which suggests a trade-off between iodine release and energy release rate. This study demonstrates that, while not all aluminized metal iodate composites show promise in biocidal application, Al-$Ca(IO_3)_2$ and Al-$LiIO_3$ composites hold promise as biocidal agents due to their combined heat and iodine release capabilities.

1. Introduction

As discussed in Part 1 of this study [1], viruses, bacteria, formulated into weapons pose serious concerns. These threats necessitate a strategy for bioagent deactivation. One effective and environmentally friendly strategy for destroying microorganism is the application iodine as a disinfectant [2–4]. Nevertheless, the high vapor pressure of iodine often renders it inefficient and inconvenient to be implemented for destroying large-scale microorganism. An alternative strategy for bioagent deactivation is the employment of energetic materials for a thermal neutralization [5–7]. However, the disadvantage of this method is the likely incomplete neutralization as the thermal event is often short. To solve the problems and take advantage of both strategies, it has been proposed that, agent defeat weapons (ADWs), a new class of energetic material that releases large amounts of strong biocides after the delivery of a thermal event, could be effective in deactivation biological materials [7–9].

Nanothermites, energetic composites typically consisting of metal fuel and oxidizer nanoparticles that undergo highly exothermic reaction upon ignition, have advantages of higher energy density and higher tunability over the conventional monomolecular CHNO energetics [10–18]. Nanothermites are particularly well-suited for application of AWDs when a suitable iodine-releasing oxidizer is used. I_2O_5 is an attractive oxidizer for this purpose due to its high iodine and oxygen content, and various studies investigated the destruction of spore forming bacteria and energy release of energetic composites containing I_2O_5 [9,19,20]. However, the practical application of I_2O_5 is limited by its hygroscopic properties. Metal iodates are potentially very attractive due to their high iodine content and strong oxidizing nature. Iodine release and combustion behavior of thermite with various metal iodates

* Corresponding author.
E-mail address: mrz@engr.ucr.edu (M.R. Zachariah).

https://doi.org/10.1016/j.combustflame.2024.113373
Received 31 December 2023; Received in revised form 1 February 2024; Accepted 11 February 2024
Available online 14 February 2024

including $Cu(IO_3)_2$, $AgIO_3$, $Bi(IO_3)_2$, $Fe(IO_3)_2$, and $Ca(IO_3)_2$, have been investigated [6,7,21,22]. These studies reveal that not all metal iodates release I_2 during decomposition.

In part 1 of this work, a systematical study was performed on the decomposition mechanism of alkali and alkaline metal iodates ($LiIO_3$, $NaIO_3$, KIO_3, $Mg(IO_3)_2$, and $Ca(IO_3)_2$), which have high iodine and oxygen content. It was demonstrated that while the iodine in $LiIO_3$, $Mg(IO_3)_2$, and $Ca(IO_3)_2$ are released as I_2 during thermal decomposition, the iodine in $NaIO_3$ and KIO_3 are trapped as metal iodide, which has limited utility as a biocide. This study reveals that not all metal iodates are promising candidates in biocidal application and provides a simple thermodynamic calculation strategy to predict the feasibility of I_2 release of metal iodates.

A key step forward to real-world application is the fabrication of these metal iodates into composites with mechanical integrity at high loading to achieve high energy density and iodine content, as well as the subsequent combustion behavior of the composites. However, the fabrication of high loading nanothermite composites is limited by processing challenges due to the high viscosity, which makes the traditional casting methods unpractical [13]. Additive manufacturing techniques such as 3D printing has attracted attention in energetic composite preparation due to its relative simplicity, customizability, and convenience [13,23–25]. Recently, free-standing composites with 90 wt% nanothermite loading were successfully prepared with 3D printing and their combustion behaviors were investigated [13,23,26–28]. Nevertheless, these studies mostly use a metal oxide as the oxidizer, and a systematic study focusing on the combustion behavior of high loading energetic composite with iodine-containing oxidizer is still lacking.

In this paper, we utilize aluminum (Al), the most commonly used fuel due to its high energy density, ready availability, and high reactivity, as the fuel to study the iodine release, ignition, and reactivity of alkali and alkaline metal iodates ($LiIO_3$, $NaIO_3$, KIO_3, $Mg(IO_3)_2$, and $Ca(IO_3)_2$) [10,12,29]. Temperature-jump time of flight mass spectrometry (T-Jump/-TOFMS) and temperature-jump ignition (T-Jump ignition) are employed to analyze the iodine release and ignition behavior of aluminized metal iodate thermites, respectively. Combustion cell measurement is utilized to determine the reactivity of these thermites. More importantly, free-standing composites with 90 wt% loading of aluminized metal iodate thermites with iodine content as high as nearly 50 wt% are successfully prepared by 3D printing and their combustion behaviors are studied by high-speed videography and pyrometry.

2. Materials and methods

2.1. Materials

$NaIO_3$ (99 %) was obtained from Alfa Aesar. $LiIO_3$ (97 %), KIO_3 (≥98 %), $MgCl_2$ (≥98 %), HIO_3 (≥99.5 %), $Ca(NO_3)_2{\cdot}4H_2O$ (≥99 %), and polyvinylidene fluoride (PVDF, average molecular weight: ~534,000) were purchased from Sigma Aldrich (Millipore Sigma). HPLC grade water, hexanes (99.9 %), N, N dimethylformamide (DMF, 99.8 %), and NaOH (≥97 %) were purchased from Fisher Scientific. METHOCEL™ F4M Hydroxypropyl Methylcellulose (HPMC) was obtained from Dow Chemical Company. Aluminum nanoparticles (Al NPs, ~50 nm, 67 wt% active) were obtained from Argonide Corporation. The active content of Al NPs was determined utilizing thermogravimetry and differential scanning calorimetry (TGA−DSC, Netsch STA449 F3 Jupiter) [13,34].

2.2. Size reduction of alkali metal iodate particles

Size of as-received alkali metal iodates was reduced via ball milling with a Retsch CryoMill operated at ambient condition. Briefly, 0.75 g alkali metal iodate, ~0.75 ml hexanes, and three steel balls (7/32″ in diameter, obtained from GlenMills) were loaded into a plastic centrifuge tube (FisherBrand 2 mL) and then milled with a Retsch CryoMill operated at ambient conditions for 30 min at a frequency of 25.0 Hz for 10 mins. After settling for ~ 5 min for cooling, the sample was ball milled again for 10 mins. This process was repeated two more times so that the total milling time was 40 mins. Then the sample was transferred into a desiccator for drying. SEM (scanning electron microscope) images of the obtained samples are shown in Figure S1.

2.3. Synthesis of alkaline metal iodates

Details for the synthesis of $Ca(IO_3)_2$ μm particle can be found in our previous publication [30]. Briefly, 236 mg $Ca(NO_3)_2{\cdot}4H_2O$, 428 mg KIO_3, three alumina balls (7/32″ in diameter, purchased from GlenMills), and 0.5 mL ethanol were added to a centrifuge tube (FisherBrand, 2 mL) and milled for 20 min at a frequency of 25.0 Hz. The resultant suspension was centrifuged at 7000 rpm for 5 min. The obtained precipitate was washed three times with 30 mL water every time and then dried in a vacuum oven overnight for water removal. The dried solid powder was baked in a tube furnace at 350 °C for 40 min in air for the removal of crystal water [22]. SEM image of the obtained $Ca(IO_3)_2$ is shown in Figure S1.

Details of synthesizing $Mg(IO_3)_2$ can be found in Part 1 [1]. SEM image of the synthesized $Mg(IO_3)_2$ is shown in Figure S1.

2.4. T-Jump ignition and TOFMS

The details of the T-Jump ignition and TOFMS tests can be found in our previous publications [11,31,32]. Briefly, Al nanoparticles and the corresponding amounts of metal iodates were physically mixed in hexane. Following 30 min of ultrasonication, a small amount of the suspension was coated on Pt wire (diameter=76 μm, 0.8–1.1 cm length, OMEGA Engineering Inc.), which was then resistively heated by a direct current voltage supply. Temperature readings of the Pt wire was obtained through calibrating with Callendar-Van Dusen equation. It is assumed the temperature of the thin coating on Pt wire is the same with temperature of the wire. A minimum of three tests were performed for every sample.

For T-Jump ignition tests, the samples were ignited inside a chamber filled with argon at 1 atm and the ignition process was recorded by a high-speed camera (Vision Research Phantom V12.1). The ignition delay time was determined from the obtained video as well as the measured wire temperature. For T-Jump TOFMS, a 70 eV electron gun ionizer was used for ionizing gas phase species produced from the sample inside the TOFMS chamber held at $\sim 10^{-6}$ Torr. For both T-Jump ignition and TOFMS, measurements were repeated at least three times.

2.5. Combustion cell measurements

Reactivity of the Al-metal iodate thermites at stoichiometric ratio were evaluated in a constant volume combustion cell (~20 cm^3), from which PV/m (P is the maximum pressure, V is the volume of the combustion cell, and m is the mass for each measurement), pressurization rate, and burn time (half width of the optical signal) were evaluated. Details of combustion cell measurements can be found in our previous studies [33,34]. 25 mg of a thermite powder was used for each measurement, which was repeated with a minimum of three times in total.

As Part 1 demonstrated, these metal iodates have two decomposition mechanisms [1]. The amount of Al and metal iodate was determined from the following equations (Eqs. (1)-(5)) for prescribing the stoichiometric ratio and are based on the decomposition paths we previously determined.

$$10Al + 3Mg(IO_3)_2 = 5Al_2O_3 + 3MgO + 3I_2 \quad (1)$$

$$10Al + 3Ca(IO_3)_2 = 5Al_2O_3 + 3CaO + 3I_2 \quad (2)$$

$$10Al + 6LiIO_3 = 5Al_2O_3 + 3Li_2O + 3I_2 \quad (3)$$

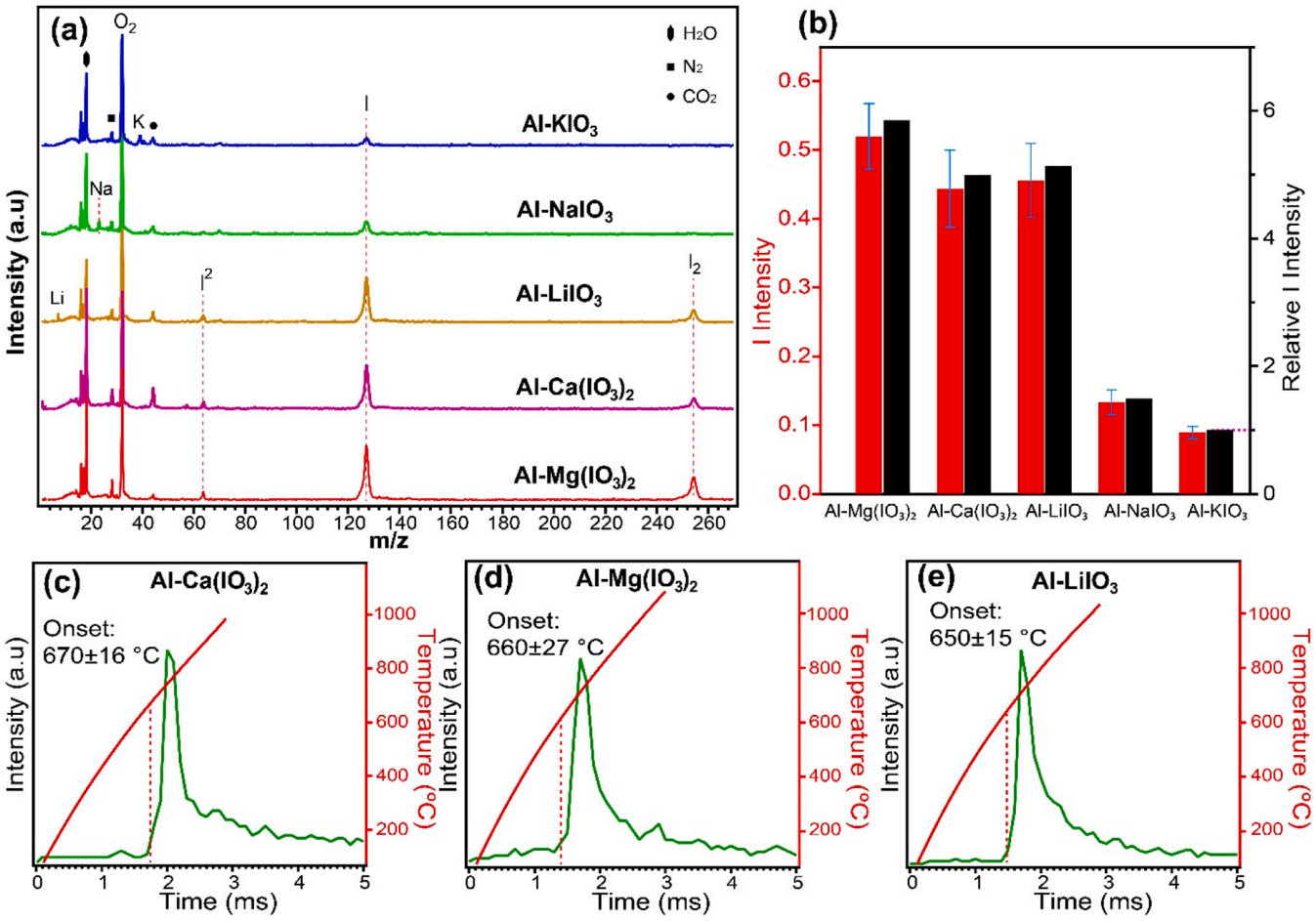

Fig. 1. T-Jump/TOFMS spectrum of alkali and alkaline metal iodate with Al (a). Most notable mass species are labeled. The measured I intensities of the iodate with Al and their relative intensity to Al-KIO_3 (b). I release over time and the corresponding heating profile of Al-$Ca(IO_3)_2$ (c), Al-$Mg(IO_3)_2$ (d), and Al-$LiIO_3$ (e). The onset I release temperature averaged over a minimum of three experiments is labeled.

$$2Al + NaIO_3 = Al_2O_3 + NaI \quad (4)$$

$$2Al + KIO_3 = Al_2O_3 + KI \quad (5)$$

2.6. Preparation of ink and direct ink writing of 90 wt% loading aluminized metal iodate composites

The details of ink preparation and direct ink writing can be found in our previous publication [13]. Briefly, 4 wt% PVDF and 6 wt% HPMC were dissolved into DMF. Metal iodate was added to the solution and the obtained suspension was ultrasonicated for 30 min. Stoichiometric amount of Al nanoparticles was then added to the suspension and the obtained sample was ultrasonicated for 30 min and magnetically stirred overnight before printing with a printer (Hyrel System 30 M). For printing, the ink was extruded through an 18-gauge needle and directly written on a preheated (~75 °C) glass substrate with a pre-designed pattern. Each layer was ensured to be dried visibly before depositing the next layer. Following printing, the obtained films were heated for 30 min at ~75 °C for removing the residual solvent. The films were then cut into ~2 cm long sticks for combustion characterizations.

2.7. Microscopic and macroscopic imaging

The details of the imaging process can be found in our previous study [35]. Generally, two imaging systems were utilized for studying the combustion behavior of the printed composites. One imaging system was macroscopic imaging system with high-speed camera (Vision Research Phantom Miro M110) and the other one was microscopic imaging system that uses high-speed camera (Vision Research Phantom VEO710L) coupled with Infinity Photo-Optical Model K2 DistaMax. For a typical measurement, one stick was placed on a stage inside an argon filled chamber that was mounted between the two imaging systems. The stick was ignited with a Joule-heated nichrome wire and the combustion process was recorded with both imaging systems.

2.8. Three-color imaging pyrometry

The details of three-color imaging pyrometry can be found in our previous publications [36–38]. Briefly, three color (red, green, and blue) intensities from the Bayer filter and their ratios were utilized for measuring the flame temperature of a sample assuming graybody emission behavior of the sample. A blackbody source (Mikron M390) was used for obtaining calibration factors. The temperature uncertainty was estimated to be nominally 200–300 K [28,38].

2.9. Scanning electron microscope

The morphology of the metal iodate micron particles as well as the cross section of the 3D-printed composites were characterized by scanning electron microscope (SEM, Thermo-Fisher Scientific NNS450).

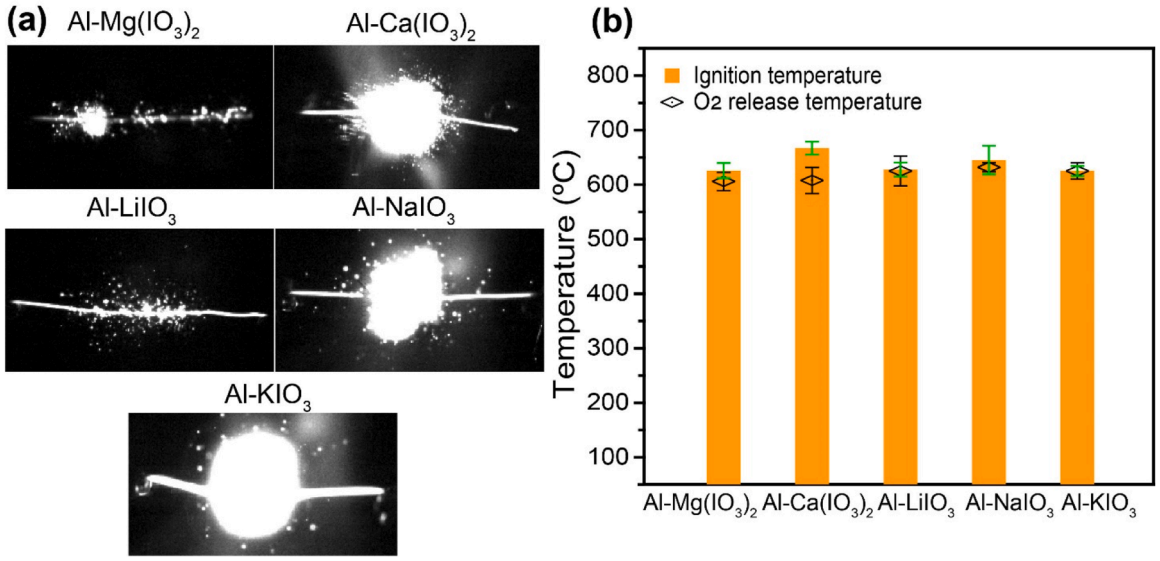

Fig. 2. T-Jump ignition snapshots of Al with alkali and alkaline metal iodate (a). O_2-release onset temperature of metal iodate estimated from T-Jump/TOFMS and T-Jump ignition temperature of metal iodate with Al.

3. Results and discussion

3.1. Time-of-flight mass spectrometry and ignition of Al-iodate thermites under rapid heating rate (~10^5 K/s)

T-Jump/TOFMS was used to analyze iodine release from the metal iodates with Al and the resulting mass spectra are shown in Fig. 1(a). As demonstrated in Part 1, alkali and alkaline metal iodates follow two different decomposition pathways: (1) decomposition into metal oxide, oxygen, and iodine, and (2) decomposition into metal iodide and oxygen [1]. $Ca(IO_3)_2$, $Mg(IO_3)_2$, and $LiIO_3$ follow pathway (1) while $NaIO_3$ and KIO_3 follow pathway (2). Therefore, upon thermal decomposition, $Ca(IO_3)_2$, $Mg(IO_3)_2$, and $LiIO_3$ release significant amount of iodine, while $NaIO_3$ and KIO_3 have minimal iodine release. Similar results are obtained with the addition of Al, where Al-$Ca(IO_3)_2$, Al-$Mg(IO_3)_2$, and Al-$LiIO_3$ release significantly higher amount of iodine than Al-$NaIO_3$ and Al-KIO_3. Semiquantitative analysis of the release behavior of I, a representative of I_2, was performed by measuring its intensity in

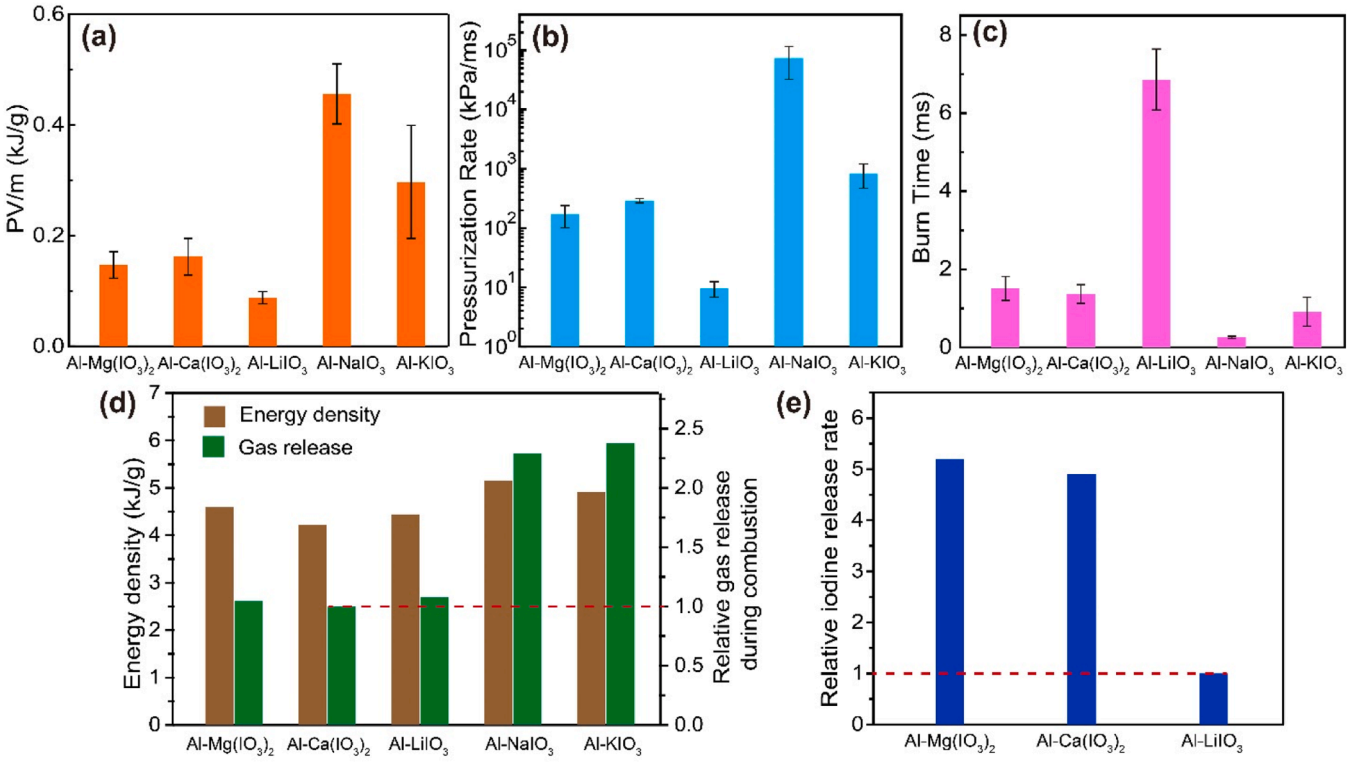

Fig. 3. PV/m (a), pressurization rata (b), and burn time (c) of Al with different metal iodates. Combustion enthalpies of Al with different metal iodates at stoichiometric ratio as well as their relative amount of gas release to Al-$Ca(IO_3)_2$ during combustion (d) [47]. Estimated relative iodine release rate of Al with different metal iodates based on the iodine release rate of Al-$LiIO_3$ (e). The iodine release rate is calculated via dividing the average iodine release intensity from TOFMS by the average burn time from pressure cell measurement.

different Al-iodate systems and relative intensity to Al-KIO_3. The results are shown in Fig. 1(b), which clearly demonstrates the iodine release difference and verifies that Al-$Ca(IO_3)_2$, Al-$Mg(IO_3)_2$, and Al-$LiIO_3$ are promising in biocidal application. One important evaluating parameter for biocidal energetics is the biocide release temperature, which is iodine in this case. Iodine release profiles of Al-$Ca(IO_3)_2$, Al-$Mg(IO_3)_2$, and Al-$LiIO_3$ displayed in Fig. 1(c)-(e) demonstrate that the iodine release temperature of these thermites are roughly the same. Such an analysis is not conduced on Al-$NaIO_3$ and Al-KIO_3 due to their low iodine release.

Ignition studies of Al with metal iodates were conducted in 1 atm argon and the representative snapshots of ignition are shown in Fig. 2 (a). These results demonstrate that all the Al-iodate systems ignite in an inert environment, although Al-$Mg(IO_3)_2$ and Al-$LiIO_3$ have less vigorous flames. Fig. 2(b) displays the O_2 release onset temperature obtained from T-Jump TOFMS of metal iodates as well as ignition temperature of Al-iodate systems. Previous studies demonstrated that polymorphic phase change in alumina (~880 K, from amorphous to γ-Al_2O_3) causes accelerated outwardly diffusion of Al and initiates the thermite reaction when gas-phase oxygen is readily available [11,39]. In the current study, O_2 release onset temperature of metal iodate and ignition temperature of Al-metal iodate are nearly the same at about 630 °C (~900 K) for all the thermites, which is slightly higher than the phase transition temperature of alumina at ~880 K, indicating the ignition is possibly limited by the availability of gaseous oxygen from metal iodate. The ignition temperature at about 630 °C is very close to the melting point of Al at 660 °C though. Therefore, it is also possible that the ignition is limited by the availability of Al from melting.

3.2. Reactivity and iodine release rate of Al-iodate thermites

Constant-volume cell measurements were conducted on the Al-iodate thermites to evaluate their reactivity and combustion characteristics including PV/m, pressurization rate, and burn time [33]. Fig. 3 displays the combustion parameters of the Al with different metal iodates. Al-$NaIO_3$ and Al-KIO_3 have significantly higher peak pressure and pressurization rate, shorter burn time as compared to Al-$Mg(IO_3)_2$, Al-$Ca(IO_3)_2$, and Al-$LiIO_3$, demonstrating their superior reactivity. These differences cannot be explained on the basis of energy density that are displayed in Fig. 3(d), which shows that differences are insignificant. It is well-known that particle size has significant effect on the reactivity of a thermite [40–42], however Figure S1 shows that the particle size is similar among these metal iodates. Further we show in Fig. 2(b), that the onset temperature of O_2 release is roughly the same for all the metal iodates, suggesting that it is unlikely the contributing factor for the reactivity difference.

Another factor that influences the PV/m and pressurization rate is the amount of gas released during the combustion process. Eq. (1–5) demonstrates that for Al-$Mg(IO_3)_2$, Al-$Ca(IO_3)_2$, and Al-$LiIO_3$, Al_2O_3, metal oxide, and I_2 are produced. The boiling point of Al_2O_3, MgO, CaO, Li_2O, and I_2 is 2967 °C, 3600 °C, 2853 °C, 2563 °C, and 184 °C, respectively [43–46], The measured flame temperature of the 3D printed composite of Al-$Ca(IO_3)_2$ and Al-$LiIO_3$ below 1700 °C, which will be discussed further in 3.3, is significantly lower than the boiling point of Al_2O_3, CaO, Li_2O. This indicates that Al_2O_3, CaO, Li_2O will remain in the condensed phase, and the only gas product is I_2. A similar temperature comparison for Al-$Mg(IO_3)_2$ cannot be performed as the flame temperature of its printed composite cannot be obtained. However, MgO has much higher boiling point and Al-$Mg(IO_3)_2$ has similar reactivity to Al-$Ca(IO_3)_2$ and Al-$LiIO_3$. Therefore it is reasonable to speculate that MgO also remains in the condensed phase during combustion. This analysis indicates that the only gaseous product during combustion for Al-$Mg(IO_3)_2$, Al-$Ca(IO_3)_2$, and Al-$LiIO_3$ is I_2. While for the combustion of Al-$NaIO_3$ and Al-KIO_3, Al_2O_3 and metal iodide are produced, and the boiling point of NaI and KI is 1304 °C and 1323 °C, respectively [44]. The measured flame temperature of 3D printed Al-$NaIO_3$ composite of ~2350 °C is much higher than the boiling point of NaI, which means NaI is gaseous during combustion. It is speculated that KI is also gaseous during combustion for Al-KIO_3 as the boiling point of KI is closed to NaI and the reactivity of Al-$NaIO_3$ and Al-KIO_3 is similar. Fig. 3(d) displays the relative amount of gas release during combustion for different thermite systems and shows Al-$NaIO_3$ and Al-KIO_3 have significantly higher amount of gas release compared to Al-$Mg(IO_3)_2$, Al-$Ca(IO_3)_2$, and Al-$LiIO_3$. This higher amount of gas release likely explains the higher PV/m and pressurization rate of Al-$NaIO_3$ and Al-KIO_3.

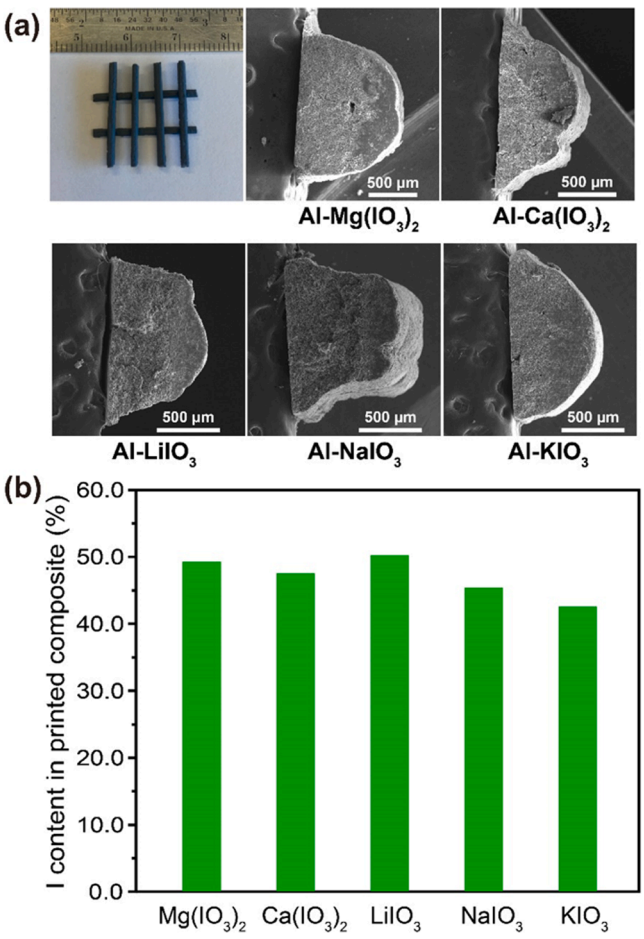

Fig. 4. SEM cross-section of the assembled composites (a). Theoretically gravimetric iodine content in the printed composite of Al with metal iodates (b). Note: Inactive content of Al is not considered for this calculation.

Al-$Mg(IO_3)_2$ and Al-$Ca(IO_3)_2$ have nearly the same reactivity as they have similar peak pressure, pressurization rate, and burn time. Al-$LiIO_3$ underperforms Al-$Mg(IO_3)_2$ and Al-$Ca(IO_3)_2$ although $LiIO_3$, $Mg(IO_3)_2$, and $Ca(IO_3)_2$ follow the same decomposition pathway and all the three thermites have similar energy density [1]. It is noteworthy that energy density of these thermite systems is calculated from the standard enthalpy of reaction at room temperature, which means endothermicity of phase change of the involved chemicals during combustion is not considered. Now a primary question arises: Why does Al-$LiIO_3$ has a lower reactivity than Al-$Mg(IO_3)_2$ and Al-$Ca(IO_3)_2$? As shown in Part 1 [1], $Mg(IO_3)_2$ and $Ca(IO_3)_2$ decompose without a noticeable melting process, while $LiIO_3$ melts at 434 °C that corresponds to a sharp endothermic peak [44]. The endothermicity of $LiIO_3$ melting leads to less heat release during the combustion process. In addition, the condense phase decomposition product of $Mg(IO_3)_2$, $Ca(IO_3)_2$, and $LiIO_3$ are MgO, CaO, and Li_2O, respectively. The melting point of Li_2O at 1438 °C is much lower than MgO and CaO at 2825 °C and 2613 °C, respectively [44]. The flame temperature is higher than the melting point of Li_2O for

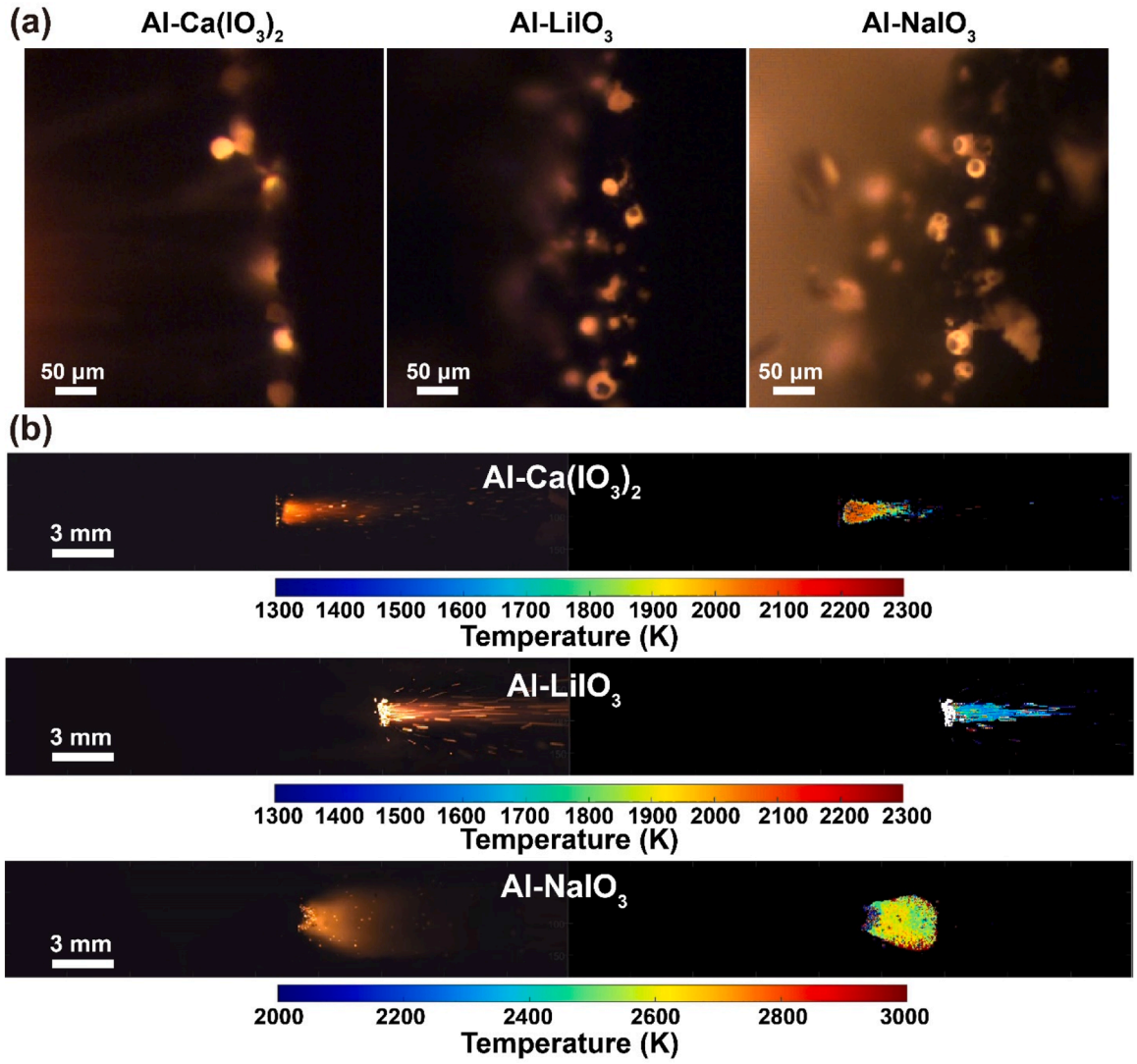

Fig. 5. Representative images from microscopic videos (a), and representative snapshots (left) as well as corresponding flame temperature maps (right) from macroscopic videos (b) of Al-Ca(IO_3)$_2$, Al-$LiIO_3$, and Al-$NaIO_3$. Note: the temperature scale bar is different for Al-$NaIO_3$ as its flame temperature is much higher than the other two composites.

Al-$LiIO_3$ but lower than the melting point of CaO and MgO in the case of Al-Mg(IO_3)$_2$ and Al-Ca(IO_3)$_2$, respectively, which will be discussed further in 3.3. This means the Li_2O melts while MgO and CaO remain as solid during the combustion process. The endothermicity of Li_2O melting will result in a further reduction in heat release from the combustion of Al-$LiIO_3$ compared to Al-Mg(IO_3)$_2$ and Al-Ca(IO_3)$_2$. Therefore, although the theoretical energy release for Al-Mg(IO_3)$_2$, Al-Ca(IO_3)$_2$, and Al-$LiIO_3$ is comparable, the actual energy release of Al-$LiIO_3$ is lower due to the endothermic nature of melting $LiIO_3$ and Li_2O during combustion. This likely explains the lower reactivity of Al-$LiIO_3$ than Al-Mg(IO_3)$_2$ and Al-Ca(IO_3)$_2$.

Iodine release rate of an energetic composite is a critical factor for the application as biocidal agent, and different iodine release rate may be preferred in different circumstances [2,21]. Fig. 3(e) displays the relative iodine release rate for thermites with significant iodine release and demonstrates that the iodine release rate of Al-Mg(IO_3)$_2$ and Ca(IO_3)$_2$ is similar and dramatically higher than Al-$LiIO_3$. This result suggests that the iodine release rate of Al-based thermite can be manipulated simply by utilizing different iodates as oxidizer, or perhaps by making mixtures.

3.3. Combustion performance of printed high loading Al-iodate composites

As mentioned above, fabrication of high particle loading composite with good mechanical properties is essential to obtain high energy density for real-world application [23]. All the Al-iodate thermites can be 3D printed into free-standing composites with 90 wt% thermite loading. The photo of a representative printed composite shows the smooth and crack-free surface and cross-section SEM images of all the printed composites are shown in Fig. 4(a). Iodine content and energy release rate are two key parameters in evaluating biocidal agent in addition to the aforementioned iodine release rate. These composites have high iodine content (nearly 50 wt%, as shown in Fig. 4(b)).

Combustion behavior of the printed composites were investigated in argon (1 atm) with high-speed microscopic imaging and macroscopic imaging coupled with pyrometry [26,35]. Interestingly, although all the Al-iodate thermites ignite in argon (1 atm), not all the printed composites can fully propagate. Al-Ca(IO_3)$_2$, Al-$LiIO_3$, and Al-$NaIO_3$ composites propagate fully, while Al-Mg(IO_3)$_2$ and Al-KIO_3 composites have incomplete propagation. The feasibility of propagation does not follow the reactivity trend or the decomposition pathway of metal iodates and is not well understood.

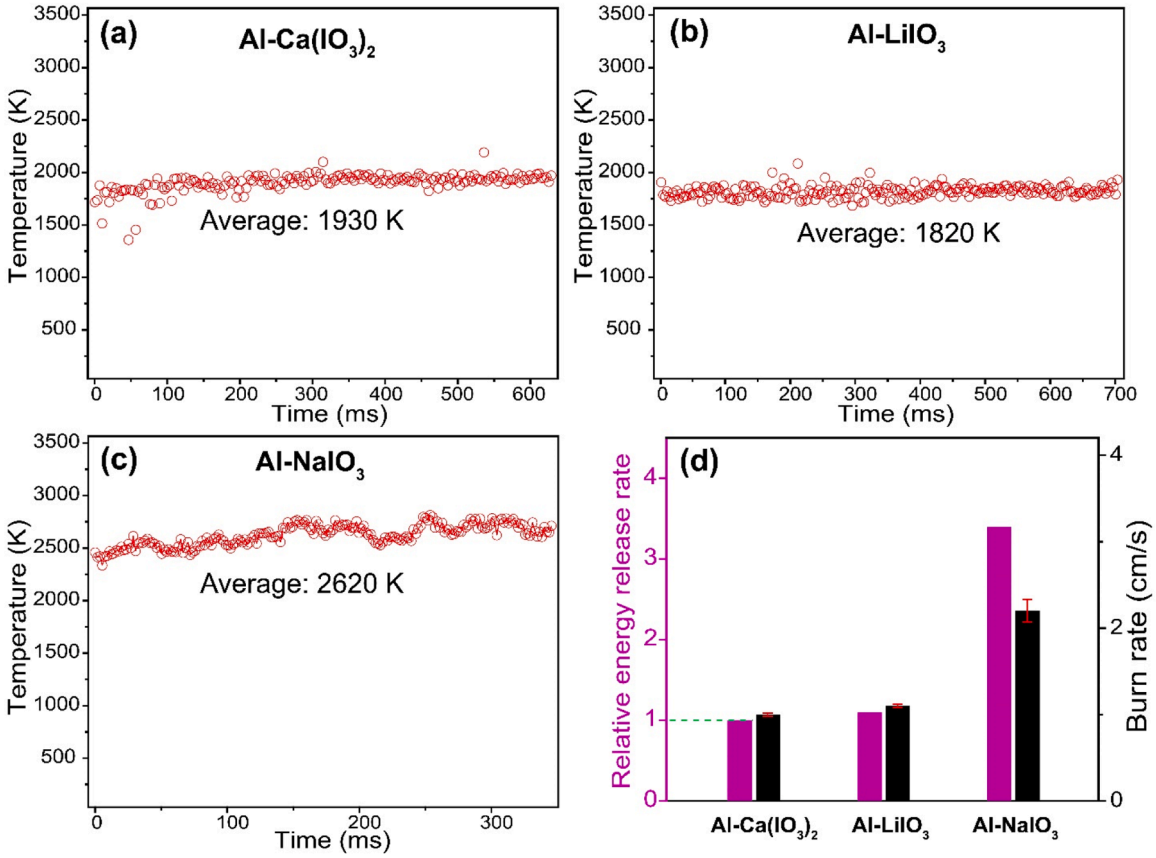

Fig. 6. Time-resolved average flame temperature from macroscopic imaging of Al-$Ca(IO_3)_2$ (a), Al-$LiIO_3$ (b), and Al-$NaIO_3$ (c). Note: Each data point represents the average temperature of the entire flame at a specific time, while the average temperature inserted is the average of all the shown data points in the figure. Burn rate and relative energy release rate of Al-$Ca(IO_3)_2$, Al-$LiIO_3$, and Al-$NaIO_3$ (d). The relative energy release rate is based on the energy release rate of Al-$Ca(IO_3)_2$.

For the composites that propagate fully in argon, the microscopic combustion characteristic is essentially the same, where Al droplet with dark cap (aluminum oxide) forms on the burning surface, as shown in Fig. 5(a). These droplets have a size of tens of micrometer and there is no significant size difference among different composites. It is worth noting that the initial Al particles incorporated into the composite is 50 nm, which suggests extensive sintering/agglomeration of Al occurs during the combustion process [26]. SEM images of the post-combustion product for Al-$Ca(IO_3)_2$, Al-$LiIO_3$, and Al-$NaIO_3$ shown in Figure S2 further confirm the similarity in agglomerate size among the three composites. SEM/EDS was utilized to analyze the element distribution of post-combustion product of Al-$Ca(IO_3)_2$ and Al-$NaIO_3$, as shown in Figure S3 and Figure S4, respectively. The presence of Na and I overlaps for Al-$NaIO_3$, suggesting the formation of NaI. While for Al-$Ca((IO_3)_2$, the presence of Ca overlaps with O instead of I, implying the formation of CaO. This is consistent to the proposed reaction in Eq. (2) and (4) based on Part 1, which demonstrates the decomposition of $Ca(IO_3)_2$ and $NaIO_3$ follow different pathway and produces CaO and NaI, respectively [1]. The same analysis from EDS is not performed for Al-$LiIO_3$ as Li is undetectable in the instrument utilized.

Three-color (RGB) pyrometry is employed to measure the temperature of the agglomerates on the burning surface from microscopic imaging as well as the flame temperature from macroscopic imaging. Figure S5 shows that the agglomerate temperature is ~2100 K for all the three composites from microscopic imaging. Fig. 5(b) displays the representative flame snapshot from macroscopic imaging of for Al-Ca $(IO_3)_2$, Al-$LiIO_3$, and Al-$NaIO_3$ and their corresponding temperature map, which demonstrate flame temperature is different among the three composites. Flame temperature profiles displayed in Fig. 6(a)-(c) show that the average flame temperature of Al-$Ca(IO_3)_2$, Al-$LiIO_3$, and Al-$NaIO_3$ is 1930 K, 1820 K, and 2620 K, respectively. The significantly higher flame temperature of Al-$NaIO_3$ is attributed to its higher reactivity, as discussed in 3.2.

In 3.2, the lower thermite reactivity of Al-$LiIO_3$ compared to Al-Mg $(IO_3)_2$ and Al-$Ca(IO_3)_2$ is attributed to the endothermicity of $LiIO_3$ and Li_2O melting with the assumption that the flame temperature of Al-$LiIO_3$ is higher than the melting point of Li_2O at 1438 °C (1711 K). The flame temperature of Al-$LiIO_3$ thermite should be higher than the printed composite at 1820 K as the composite has 10 % polymer binder that reduces the overall energy density. This is consistent with our proposition that Li_2O melts during the combustion of the thermite and the endothermicity contributes to the lower reactivity of Al-$LiIO_3$. As for Al-$Ca(IO_3)_2$, the melting point of CaO at 2613 °C (2886 K) is almost 1000 K higher than the flame temperature of the printed Al-$Ca(IO_3)_2$ composite, which means the flame temperature of Al-$Ca(IO_3)_2$ thermite is unlikely to be sufficiently high for melting CaO.

A comparison of the combustion performance of the printed composites is displayed in Fig. 6(d), where the burn rate is obtained from the macroscopic imaging and the relative energy release rate is estimated based on Equation S1 [27]. Al-$Ca(IO_3)_2$ and Al-$LiIO_3$ have nearly the same burn at ~1 cm/s, which is about half of the burn rate of Al-$NaIO_3$ at ~2.2 cm/s. The estimated energy release rate of Al-$NaIO_3$ is much higher than Al-$Ca(IO_3)_2$ and Al-$LiIO_3$, consistent with the aforementioned analysis from pressure cell tests that demonstrate Al-$NaIO_3$ has significantly higher reactivity than Al-$Ca(IO_3)_2$ and Al-$LiIO_3$. This means the printed composite of Al-$NaIO_3$ is more effective in releasing heating than Al-$Ca(IO_3)_2$ and Al-$LiIO_3$. However, as discussed in 3.1, Al-$NaIO_3$ only releases minimal amount of iodine compared with Al-$Ca(IO_3)_2$ and Al-$LiIO_3$, implying there is a trade-off between iodine release and heat release among these printed composites.

4. Conclusions

In this part 2 paper, we conduct a systematic exploration of the iodine release, ignition, and reactivity of aluminized thermites containing alkali and alkaline metal iodate ($LiIO_3$, $NaIO_3$, KIO_3, $Mg(IO_3)_2$, and $Ca(IO_3)_2$) and the combustion behavior aluminized metal iodate composites. T-Jump TOFMS demonstrates that Al-$Mg(IO_3)_2$, Al-$Ca(IO_3)_2$, and Al-$LiIO_3$ release significant amount of iodine at roughly the same temperature, while $NaIO_3$ and Al-KIO_3 have minimal iodine release. Combustion cell analysis demonstrates the reactivity of Al-$Mg(IO_3)_2$, Al-$Ca(IO_3)_2$, and Al-$LiIO_3$ underperforms Al-$NaIO_3$ and Al-KIO_3, suggesting the trade-off between reactivity and iodine release. Incorporating data from both T-Jump TOFMS and combustion cell, we find that Al-$Mg(IO_3)_2$ and Al-$Ca(IO_3)_2$ have a similar iodine release rate, which is significantly higher than Al-$LiIO_3$. Free-standing Al-metal iodate composites with 90 wt% thermite loading and nearly 50 wt% iodine content are successfully prepared by 3D printing and their combustion behavior is characterized utilizing high-speed videography and pyrometry. It is found that only Al-$Ca(IO_3)_2$, Al-$LiIO_3$ and Al-$NaIO_3$ completely propagate in an inert environment and they display analogous microscopic combustion behavior characterized by spherical droplets formation on the burning surface. Comparing the macroscopic combustion behavior of the Al-$Ca(IO_3)_2$ and Al-$LiIO_3$ composites, minimal difference in propagation rate and flame temperature is identified, leading to comparable energy release rates. In contrast, the higher propagation rate and flame temperature of Al-$NaIO_3$ composite result in a significantly higher energy release rate than Al-$Ca(IO_3)_2$ and Al-$LiIO_3$, highlighting the trade-off between iodine release and heat release. This study reveals that while not all aluminized metal iodate composites are potential candidates in biocidal application, Al-$Ca(IO_3)_2$ and Al-$LiIO_3$ composites are promising biocidal agents due to both heat and iodine release.

Novelty and significance statement

Energetic materials capable of releasing substantial amounts of iodine alongside a thermal event has been proposed to be effective in deactivating bioagent. Ideally, in-situ formation of molecular iodine from an oxidizer of the energetic materials is preferred to maintain high energy density. Metal iodates are attractive for this purpose due to their high oxygen and iodine content. While various studies have explored the combustion behavior of metal iodates as oxidizer, a key step forward to real-world application is still lacking. This work not only studies the iodine release and combustion behavior of aluminized metal iodates but also investigates the combustion characteristics of the fabricated free-standing 90 wt% loading aluminized metal iodate composites with high iodine content.

Author contributions statement

Y.W designed and performed experiment, analyzed data and wrote the paper. G.P performed experiment and reviewed the paper. E.H performed characterization and reviewed the paper. H.W performed experiment and reviewed the paper. M.R.Z investigated and supervised the research, reviewed and edited the paper.

Declaration of competing interest

The authors declare that they have no known competing financial interests or personal relationships that could have appeared to influence the work reported in this paper.

Acknowledgments

This work was supported by a DTRA-URA Center for Materials Science in Extreme Environments.

Supplementary materials

Supplementary material associated with this article can be found, in the online version, at doi:10.1016/j.combustflame.2024.113373.

References

[1] Y. Wang, K. Shi, G. Issac Paul, P. Biswas, M.R. Zachariah, Combustion behavior of aluminized metal iodate composites. Part 1: decomposition mechanism of metal iodates, Combust. Flame (2024).
[2] J. Chang, G. Zhao, X. Zhao, C. He, S. Pang, J.M. Shreeve, New promises from an old friend: iodine-rich compounds as prospective energetic biocidal agents, Acc. Chem. Res. 54 (2021) 332–343.
[3] M.J. Gray, W.-Y. Wholey, U. Jakob, Bacterial responses to reactive chlorine species, Annu. Rev. Microbiol. 67 (2013) 141–160.
[4] M. Wheelis, Deadly Cultures: Biological Weapons Since 1945, Harvard University Press, 2006.
[5] T. Wu, A. SyBing, X. Wang, M.R. Zachariah, Aerosol synthesis of phase pure iodine/iodic biocide microparticles, J. Mater. Res. 32 (2017) 890–896.
[6] X. Hu, J.B. DeLisio, X. Li, W. Zhou, M.R. Zachariah, Direct deposit of highly reactive Bi(IO3)3- polyvinylidene fluoride biocidal energetic composite and its reactive properties, Adv. Eng. Mater. 19 (2017) 1500532.
[7] K.T. Sullivan, N.W. Piekiel, S. Chowdhury, C. Wu, M.R. Zachariah, C.E. Johnson, Ignition and combustion characteristics of nanoscale Al/AgIO3: a potential energetic biocidal system, Combust. Sci. Technol. 183 (2010) 285–302.
[8] T. Kaiho, Iodine Chemistry and Applications, John Wiley & Sons, 2014.
[9] F. Xu, P. Biswas, G. Nava, J. Schwan, D.J. Kline, M.C. Rehwoldt, L. Mangolini, M. R. Zachariah, Tuning the reactivity and energy release rate of I2O5 based ternary thermite systems, Combust. Flame 228 (2021) 210–217.
[10] W. Zhao, H. Ren, T. Yan, Y. Ou, Q. Jiao, H. Wang, D.J. Kline, M.R. Zachariah, Tailoring energy release of nano-Si based thermites via incorporation of Ti nanoparticles, Chem. Eng. J. 396 (2020) 124559.
[11] W. Zhou, J.B. DeLisio, X. Wang, M.R. Zachariah, Reaction mechanisms of potassium oxysalts based energetic composites, Combust. Flame 177 (2017) 1–9.
[12] G. Jian, N.W. Piekiel, M.R. Zachariah, Time-resolved mass spectrometry of nano-Al and nano-Al/CuO thermite under rapid heating: a mechanistic study, J. Phys. Chem. C 116 (2012) 26881–26887.
[13] H. Wang, J. Shen, D.J. Kline, N. Eckman, N.R. Agrawal, T. Wu, P. Wang, M. R. Zachariah, Direct writing of a 90 wt% particle loading nanothermite, Adv. Mater. 31 (2019) 1806575.
[14] W. He, P.-J. Liu, G.-Q. He, M. Gozin, Q.-L. Yan, Highly Reactive metastable intermixed composites (MICs): preparation and characterization, Adv. Mater. 30 (2018) 1706293.
[15] Y. Zhu, X. Zhou, J. Xu, X. Ma, Y. Ye, G. Yang, K. Zhang, In situ preparation of explosive embedded CuO/Al/CL20 nanoenergetic composite with enhanced reactivity, Chem. Eng. J. 354 (2018) 885–895.
[16] N.H. Yen, L.Y. Wang, Reactive metals in explosives, Propellants Explos. Pyrotech. 37 (2012) 143–155.
[17] M. Comet, C. Martin, M. Klaumünzer, F. Schnell, D. Spitzer, Energetic nanocomposites for detonation initiation in high explosives without primary explosives, Appl. Phys. Lett. 107 (2015) 243108.
[18] A. Prakash, A.V. McCormick, M.R. Zachariah, Synthesis and reactivity of a super-reactive metastable intermolecular composite formulation of Al/KMnO4, Adv. Mater. 17 (2005) 900–903.
[19] B.R. Clark, M.L. Pantoya, The aluminium and iodine pentoxide reaction for the destruction of spore forming bacteria, Phys. Chem. Chem. Phys. 12 (2010) 12653–12657.
[20] K.S. Martirosyan, L. Wang, D. Luss, Novel nanoenergetic system based on iodine pentoxide, Chem. Phys. Lett. 483 (2009) 107–110.
[21] H. Wang, G. Jian, W. Zhou, J.B. DeLisio, V.T. Lee, M.R. Zachariah, Metal iodate-based energetic composites and their combustion and biocidal performance, ACS Appl. Mater. Interfaces 7 (2015) 17363–17370.
[22] H. Wang, D.J. Kline, M. Rehwoldt, M.R. Zachariah, Ignition and combustion characterization of Ca(IO3)2-based pyrotechnic composites with B, Al, and Ti, Propellants Explos. Pyrotech. 43 (2018) 977–985.
[23] J. Shen, H. Wang, D.J. Kline, Y. Yang, X. Wang, M. Rehwoldt, T. Wu, S. Holdren, M. R. Zachariah, Combustion of 3D printed 90 wt% loading reinforced nanothermite, Combust. Flame 215 (2020) 86–92.
[24] F.D. Ruz-Nuglo, L.J. Groven, 3-D printing and development of fluoropolymer based reactive inks, Adv. Eng. Mater. 20 (2018) 1700390.
[25] S. Ghosh, S.T. Parker, X. Wang, D.L. Kaplan, J.A. Lewis, Direct-write assembly of microperiodic silk fibroin scaffolds for tissue engineering applications, Adv. Funct. Mater. 18 (2008) 1883–1889.
[26] Y. Wang, E. Hagen, P. Biswas, H. Wang, M.R. Zachariah, Imaging the combustion characteristics of Al, B, and Ti composites, Combust. Flame 252 (2023) 112747.
[27] H. Wang, Y. Wang, M. Garg, J.S. Moore, M.R. Zachariah, Unzipping polymers significantly enhance energy flux of aluminized composites, Combust. Flame 244 (2022) 112242.
[28] H. Wang, D.J. Kline, M.C. Rehwoldt, M.R. Zachariah, Carbon fibers enhance the propagation of high loading nanothermites: in situ observation of microscopic combustion, ACS Appl. Mater. Interfaces (2021).
[29] R.A. Yetter, G.A. Risha, S.F. Son, Metal particle combustion and nanotechnology, Proc. Combust. Inst. 32 (2009) 1819–1838.

[30] H. Wang, J.B. DeLisio, T. Wu, X. Wang, M.R. Zachariah, One-step solvent-free mechanochemical synthesis of metal iodate fine powders, Powder Technol. 324 (2018) 62–68.
[31] Y. Wang, H. Wang, F. Xu, P. Ghildiyal, M.R. Zachariah, Effect of alkali metal perchlorate and iodate type on boron ignition: the role of oxidizer phase change, Chem. Eng. J. 446 (2022) 136786.
[32] M.C. Rehwoldt, Y. Wang, F. Xu, P. Ghildiyal, M.R. Zachariah, High-temperature interactions of metal oxides and a PVDF binder, ACS Appl. Mater. Interfaces (2022).
[33] K. Sullivan, M. Zachariah, Simultaneous pressure and optical measurements of nanoaluminum thermites: investigating the reaction mechanism, J. Propuls. Power 26 (2010) 467–472.
[34] K. Sullivan, G. Young, M.R. Zachariah, Enhanced reactivity of nano-B/Al/CuO MIC's, Combust. Flame 156 (2009) 302–309.
[35] H. Wang, B. Julien, D. Kline, Z. Alibay, M. Rehwoldt, C. Rossi, M. Zachariah, Probing the reaction zone of nanolaminates at ~μs time and ~μm spatial resolution, J. Phys. Chem. C 124 (2020) 13679–13687.
[36] H. Wang, D.J. Kline, M.R. Zachariah, In-operando high-speed microscopy and thermometry of reaction propagation and sintering in a nanocomposite, Nat. Commun. 10 (2019) 3032.
[37] R.J. Jacob, D.J. Kline, M.R. Zachariah, High speed 2-dimensional temperature measurements of nanothermite composites: probing thermal vs. gas generation effects, J. Appl. Phys. 123 (2018) 115902.
[38] D.J. Kline, Z. Alibay, M.C. Rehwoldt, A. Idrogo-Lam, S.G. Hamilton, P. Biswas, F. Xu, M.R. Zachariah, Experimental observation of the heat transfer mechanisms that drive propagation in additively manufactured energetic materials, Combust. Flame 215 (2020) 417–424.
[39] M.A. Trunov, M. Schoenitz, E.L. Dreizin, Effect of polymorphic phase transformations in alumina layer on ignition of aluminium particles, Combust. Theory Model. 10 (2006) 603–623.
[40] K.T. Sullivan, J.D. Kuntz, A.E. Gash, The role of fuel particle size on flame propagation velocity in thermites with a nanoscale oxidizer, Propellants Explos. Pyrotech. 39 (2014) 407–415.
[41] Y. Huang, G.A. Risha, V. Yang, R.A. Yetter, Effect of particle size on combustion of aluminum particle dust in air, Combust. Flame 156 (2009) 5–13.
[42] D.S. Sundaram, V. Yang, V.E. Zarko, Combustion of nano aluminum particles (Review), Combust. Explos. Shock Waves 51 (2015) 173–196.
[43] Y. Chen, D.R. Guildenbecher, K.N.G. Hoffmeister, M.A. Cooper, H.L. Stauffacher, M.S. Oliver, E.B. Washburn, Study of aluminum particle combustion in solid propellant plumes using digital in-line holography and imaging pyrometry, Combust. Flame 182 (2017) 225–237.
[44] W.M. Haynes, CRC Handbook of Chemistry and Physics, 95th Edition, CRC Press, Hoboken, 2014.
[45] R.C. Ropp, Group 16 (O, S, Se, Te) alkaline earth compounds. Encycl. Alkaline Earth Compd., Elsevier, 2013, pp. 105–197.
[46] G.F. Kessinger, A.R. Jurgensen, D.M. Missimer, J.S. Morrell, The high-temperature chemical reactivity of Li2O, Nucl. Technol. 171 (2010) 108–122.
[47] Materials Project, (n.d.). https://materialsproject.org/.